University of Massachusetts Medical School

eScholarship@UMMS

RNA Therapeutics Institute Publications   RNA Therapeutics Institute

2016-10-01

Exosome-mediated Delivery of Hydrophobically Modified siRNA for Huntingtin mRNA Silencing

Marie C. Didiot
University of Massachusetts Medical School

Et al.

Let us know how access to this document benefits you.

Follow this and additional works at: https://escholarship.umassmed.edu/rti_pubs

Part of the Cell and Developmental Biology Commons, Genetics and Genomics Commons, Molecular Biology Commons, Neuroscience and Neurobiology Commons, and the Therapeutics Commons

Exosome-mediated Delivery of Hydrophobically Modified siRNA for Huntingtin mRNA Silencing

Marie-Cécile Didiot[1,2], Lauren M Hall[1,3], Andrew H Coles[1,2], Reka A Haraszti[1,2], Bruno MDC Godinho[1,2], Kathryn Chase[1,3], Ellen Sapp[4], Socheata Ly[1,2], Julia F Alterman[1,2], Matthew R Hassler[1,2], Dimas Echeverria[1,2], Lakshmi Raj[5], David V Morrissey[5], Marian DiFiglia[4], Neil Aronin[1,3] and Anastasia Khvorova[1,2]

[1]RNA Therapeutics Institute, University of Massachusetts Medical School, Worcester, Massachusetts, USA; [2]Department of Molecular Medicine, University of Massachusetts Medical School, Worcester, Massachusetts, USA; [3]Department of Medicine, University of Massachusetts Medical School, Worcester, Massachusetts, USA; [4]Institute for Neurodegenerative Disease, Massachusetts General Hospital, Charlestown, Massachusetts, USA; [5]Novartis Institutes for Biomedical Research Inc., Cambridge, Massachusetts, USA

Delivery represents a significant barrier to the clinical advancement of oligonucleotide therapeutics for the treatment of neurological disorders, such as Huntington's disease. Small, endogenous vesicles known as exosomes have the potential to act as oligonucleotide delivery vehicles, but robust and scalable methods for loading RNA therapeutic cargo into exosomes are lacking. Here, we show that hydrophobically modified small interfering RNAs (hsiRNAs) efficiently load into exosomes upon co-incubation, without altering vesicle size distribution or integrity. Exosomes loaded with hsiRNAs targeting *Huntingtin* mRNA were efficiently internalized by mouse primary cortical neurons and promoted dose-dependent silencing of *Huntingtin* mRNA and protein. Unilateral infusion of hsiRNA-loaded exosomes, but not hsiRNAs alone, into mouse striatum resulted in bilateral oligonucleotide distribution and statistically significant bilateral silencing of up to 35% of *Huntingtin* mRNA. The broad distribution and efficacy of hsiRNA-loaded exosomes delivered to brain is expected to advance the development of therapies for the treatment of Huntington's disease and other neurodegenerative disorders.

INTRODUCTION

A broad range of human diseases, including cancer or neurodegeneration, can be treated *via* the silencing of specific genes using small oligonucleotides. Oligonucleotide therapeutics (ONTs) are a new class of drugs, distinguished by targeting RNA or DNA, and thus preventing expression of the protein responsible for the disease phenotype. Expansion of CAG repeats in the *huntingtin* gene (*HTT*) causes Huntington's disease (HD),[1] a dominant neurodegenerative disorder characterized by progressive abnormal movements, cognitive deficit, and depression.[2,3] The mechanism of pathogenesis remains poorly understood,[3] with the striatum and cortex being primary affected.[2] Direct *HTT* mRNA targeting with ONTs and partial silencing of both wild-type and mutant *HTT* alleles in striatum and cortex is a promising strategy for HD treatment.[4–7]

One class of ONTs is small interfering RNA (siRNA), short RNA duplexes that are comprised of a passenger (sense) and a guide (antisense) strand. Upon cellular uptake, the guide strand is loaded into an RNA Induced Silencing Complex (RISC) capable of cleaving its complementary target mRNA. Loaded RISC is a multiple-turnover enzymatic complex. Recent studies estimate that as few as 25–100 active RISCs can provide efficient long-term silencing *in vitro* and *in vivo*.[8,9] Despite significant promise, the clinical utility of siRNA for the treatment of neurodegenerative disorders is hampered by inefficient CNS tissue delivery and distribution.[10,11]

Hydrophobically modified siRNAs (hsiRNAs) are asymmetric oligonucleotides with chemical modifications that improve stability and promote cellular internalization.[12] A cholesterol moiety, conjugated to the 3′ end of the passenger strand, enables rapid membrane association, and the single-stranded phosphorothioate tail promotes cellular internalization by a mechanism similar to that used by conventional antisense oligonucleotides.[13] We have recently demonstrated that these compounds efficiently bind cellular membranes, enter cells, and induce potent gene silencing.[14] A bolus intrastriatal injection of *Htt*-targeting hsiRNA induces local *Htt* mRNA silencing; however, this activity is limited to ipsilateral side of the brain, as significant hydrophobicity drives hsiRNA retention around the site of injection.[14]

Exosomes have recently emerged as a promising vehicle for siRNA delivery. These endogenously produced, extracellular vesicles mediate intercellular communication by transferring lipids, proteins, and RNAs between cells.[15,16] Exosomes have been isolated from diverse body fluids, including cerebrospinal fluid (CSF), and play a crucial role in physiological and pathological processes.[15,16] Exploiting the natural properties of exosomes, particularly the ability to functionally transport small RNAs,[17–19] might offer an

alternative solution for improving oligonucleotide brain distribution and neuronal uptake.[20–27] Electroporation or loading of synthetic siRNAs and microRNAs into naturally secreted extracellular vesicles has been shown to promote cellular uptake and target gene silencing.[28–30] Yet a lack of robust, scalable methods to load exosomes with artificial siRNAs has impeded development of exosomes as a viable delivery vehicle.

Here, we decided to explore if the membrane binding ability of hsiRNA could be exploited to enable exosomal loading with the synthetic siRNAs. We demonstrate that simple co-incubation of hsiRNAs with exosomes is an efficient method for productive and controlled loading of exosomes with chemically synthesized oligonucleotide cargo. Exosomes loaded with hsiRNA^{HTT} targeting *Htt* mRNA mediate nontoxic internalization of hsiRNA^{HTT} and dose-dependent silencing of *Htt* mRNA and protein in primary cortical neurons, a cell type that is traditionally difficult to transfect.[31] Unilateral infusion of hsiRNA^{HTT}-loaded exosomes into the striatum results in bilateral distribution of hsiRNA^{HTT} in both striatal and cortical regions, associated with statistically significant bilateral silencing of *Htt* mRNA in the striatum. Thus, our data provide a path toward the use of exosomes for delivery of ONTs to treat neurodegenerative disorders.
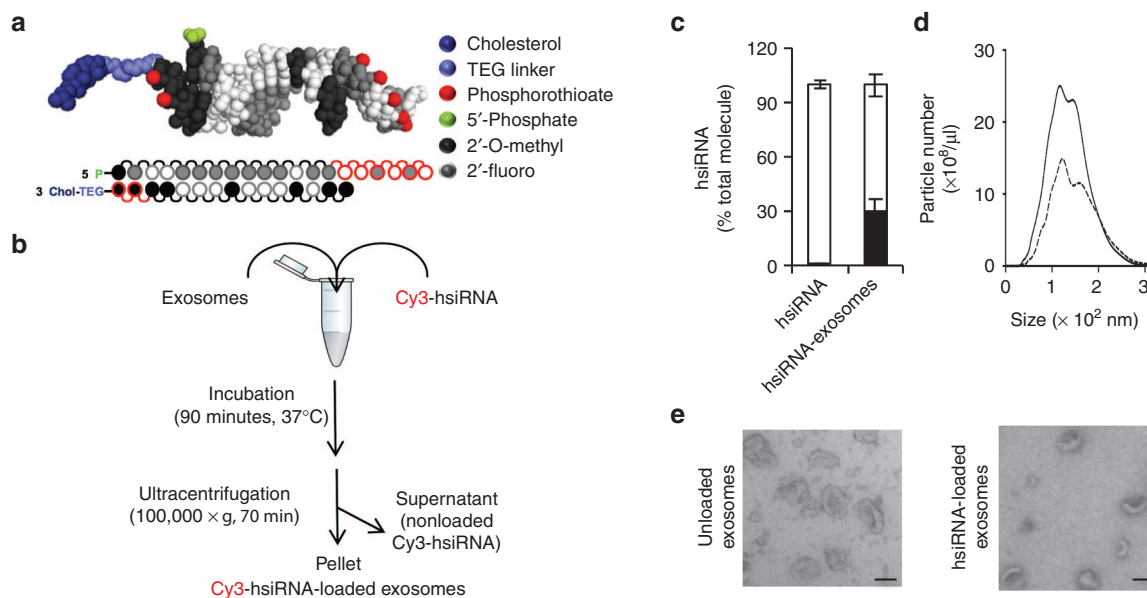
RESULTS

hsiRNAs efficiently load into exosomes

hsiRNAs are asymmetric siRNAs, with a short duplex region (12–15 base pairs) and a single-stranded, fully phosphorothioated tail, where all pyrimidines are modified with 2′-fluoro or 2′-*O*-methyl (providing stabilization and avoidance of a protein kinase R response[32]). The 3′ end of the passenger strand is conjugated to a bioactive hydrophobic conjugate (TEG–Cholesterol).[12] The cholesterol enables quick membrane

association, while the single-stranded phosphorothioated tail is essential for cellular internalization by a mechanism similar to that used by conventional antisense oligonucleotides (Ly *et al.*, 2016; In review) (**Figure 1a** and **Table 1**). The sequences and chemical modification patterns of compounds used in this study are shown in **Table 1**. The ability of hsiRNAs to interact with cellular membranes prompted us to test whether hsiRNAs could efficiently load into exosomes. We purified exosomes by differential centrifugation of conditioned media from glioblastoma U87 cells (**Supplementary Figure S1a**).[33] Nanoparticle tracking analysis and electron microscopy showed that the purified exosomes are homogeneous in size, with an average diameter of ~140 nm (**Figure 1**, **Supplementary Figure S1b** and **Table 2**), and exhibit a characteristic cup shape[33] (**Supplementary Figure S1c**). Size exclusion chromatography of exosomes and of conditioned media before and after ultracentrifugation showed that differential centrifugation precipitates most vesicles of this size (**Supplementary Figure S1d**).

Freshly purified U87-derived exosomes were incubated with 10 μmol/l Cy3-hsiRNA^{HTT} (**Figure 1a,b**). hsiRNA^{HTT} was recently identified in a screen and targets position 10150 of the human *HTT* mRNA sequence.[14] Ultracentrifugation of the Cy3-hsiRNA^{HTT}-exosome mixture generated a bright red pellet, confirming the association of fluorescently labeled hsiRNA with the high-molecular-weight vesicles (**Figure 1b,c**, **Supplementary Figure S2b**). A Cy3-hsiRNA^{HTT} pellet was observed only in the presence of exosomes (**Supplementary Figure S2b**), indicating the absence of detectable non-loaded hsiRNA aggregation. Consistent with its role in promoting membrane interactions, the cholesterol moiety was required for loading of Cy3-hsiRNA^{HTT} into exosomes and non-cholesterol conjugates hsiRNAs did not associate with

Figure 1 Efficient loading of exosomes with hsiRNAs. (**a**) hsiRNA^{HTT} schematic and PyMOL model. (**b**) Flowchart of exosome loading procedure: co-incubation of Cy3-hsiRNA and exosomes results in Cy3-hsiRNA-loaded exosomes that pellet by ultracentrifugation. (**c**) Bar graphs showing the percent of Cy3-hsiRNA or Cy3-hsiRNA-exosomes in the pellet (black) and supernatant (white) after ultracentrifugation (*n* = 3; mean ± SD). (**d**) hsiRNA loading does not affect exosome size distribution (nonloaded exosomes, solid line; hsiRNA-loaded exosomes, dashed line). (**e**) Electron microscopy of exosomes in the absence (left) or presence (right) of hsiRNA. Exosomes remain intact when loaded with hsiRNA (scale bar = 100 nm). hsiRNA, hydrophobically modified small interfering RNA.

Table 1 Table describing hsiRNA target, sequences and modifications, and PNA strand

| Target | Compounds | | Strand | Sequence 5′–3′ | Conjugate |
	Name	Type			
Nontargeting control	hsiRNA^{NTC}	hsiRNA	S	mA.mC.A.A.mU.A.mC.G.A.mU#mU#Ma	Cholesterol
			AS	PmU.A.A.fU.fC.G.fU.A.fU.fU.fU.G.mU#mC#A#A#mU#mC#A	
Huntingtin	siRNA^{HTT}	siRNA	S	mC.mA.G.mU.A.A.A.mG.A.G.A.mU.mU#mA#Ma	None
			AS	PmU.fU.A.A.fU.fC.fU.fC.fU.fU.fU.A.fC.fU#G#A#fU#A#fU#A	
Huntingtin	hsiRNA^{HTT}	hsiRNA	S	mC.mA.G.mU.A.A.A.mG.A.G.A.mU.mU#mA#Ma	Cholesterol
			AS	PmU.fU.A.A.fU.fC.fU.fC.fU.fU.fU.A.fC.fU#G#A#fU#A#fU#A	
sFlt-1	hsiRNA^{sFlt1}	hsiRNA	S	Not published	Cholesterol
			AS	Not published	
Antisense hsiRNA^{HTT}	PNA^{HTT}	PNA	S	Cy3-OO-*T*A*T*A*T*C*A*G*T*A*A*A*T*A*G*A*T*T*A*A	None

m, 2′-O-methyl; f, 2′-fluoro; #, phosphorothioate; P, phosphate; *, peptidyl interaction; hsiRNA, hydrophobically modified small interfering RNA; PNA, peptide nucleic acid; S, sense; AS, antisense.

Table 2 Table describing the characteristics of nonloaded and hsiRNA-loaded exosomes, including surface charge (Zetasizer, Malvern)

	Unloaded exosomes	hsiRNA-loaded exosomes
Particles number (µl)	10^9	10^9
hsiRNAs (molecules/vesicle)	—	1,000–3,000
Mean size (nm)	141	145
Zeta potential (mV)	−13	−32

hsiRNA, hydrophobically modified small interfering RNA.

exosomes (**Supplementary Figure S2c**). The majority of hsiR-NA^{HTT}-loaded exosomes suspended in phosphate-buffered saline (PBS) were stable, with about 80% of Cy3 fluorescence signal remaining associated with the vesicles after repetitive ultracentrifugation (**Supplementary Figure S2a**). About 10–50% of the hsiRNA in solution associated with exosomes; this estimation was based on the concentration of hsiRNA remaining in solution after loading (relative pellet and solution fluorescence). We estimate that ~1,000 to 3,000 hsiRNAs associate with each exosome with 3,000 being close to saturation (**Figure 1c** and **Table 2**).

Exosomes loaded with hsiRNAs were similar in size (**Figure 1d**) and shape (**Figure 1e**) to unloaded exosomes. Electron microscopy of exosomes loaded with biotinylated hsiRNAs and labeled with streptavidin-gold revealed that hsiRNAs are present both on the surface and in the lumen of hsiRNA-loaded exosomes (**Supplementary Figure S3**). We observed a significantly higher percent with gold particles on the outside and the inside of exosomes incubated with biotin-hsiRNAs compared to exosomes unloaded with hsiRNA. These data suggest that while the majority of hsiRNAs bind the exosome membrane, some are present in the lumen of exosomes as well. Consistent with the presence of hsiRNAs on the surface of exosomes, the surface charge (zeta potential) of the hsiRNA-loaded exosomes was lower than that of unloaded exosomes (**Table 2**). Taken together, these data indicate that the cholesterol moiety promotes efficient and stable loading of chemically synthesized siRNAs onto exosomes by simple co-incubation without disrupting the overall vesicle integrity.

hsiRNA-loaded exosomes efficiently enter into primary neurons and induce silencing of both *Htt* mRNA and HTT protein

To determine if hsiRNA-loaded exosomes efficiently enter primary cortical neurons, we prepared fluorescently labeled hsiR-NA^{HTT}-loaded exosomes, in which hsiRNA^{HTT} was labeled with Cy3 (red), and exosomes were labeled with the lipophilic dye PKH67 (green). hsiRNA^{HTT}-loaded exosomes were added to the culture medium (**Figure 2a**, **Supplementary Figure S4**), and the levels of intracellular fluorescence intensity were monitored by confocal microscopy. We prepared a PKH67 sample (without exosomes) and samples of PKH67-labeled exosomes in the same way. The PKH67 control did not produce any detectable cellular labeling compared to PKH67-labeled exosomes (**Supplementary Figure S4**, top and middle panel). The kinetics of internalization of exosomes, loaded or not with hsiRNA^{HTT}, were comparable, indicating that the incorporation of oligonucleotide cargo did not significantly interfere with the exosomal uptake properties (**Supplementary Figure S4**, middle panel). To evaluate the impact of exosomal loading on the kinetics and efficiency of hsiRNA uptake, primary neurons were treated with nonloaded and exosome-loaded Cy3-hsiRNAs. We found that hsiRNA^{HTT}-loaded exosomes enter primary neurons (**Figure 2a,b**). Although there might be a short delay early in the kinetic, by 6 hours, there is no more difference detected between hsiRNA^{HTT} and hsiRNA^{HTT}-exosome (**Figure 2a,b**, **Supplementary Figure S4**, lower panel).

We measured colocalization of PKH67 (exosomes marker) and Cy3 (hsiRNA marker) and observed that >62% of fluorescence colocalized 24 hours after cells were treated with hsiR-NA^{HTT}-loaded exosomes. This indicates that significant fraction of hsiRNA^{HTT}-loaded exosomes remains stable inside the cells.

To evaluate the impact of hsiRNA^{HTT}-loaded exosomes concentration on efficiency of hsiRNA^{HTT} neuronal uptake, the neuronal Cy3-hsiRNA was measured at 4 days post-treatment (high-performance liquid chromatography (HPLC), see Materials and Methods) (**Figure 2c**). The efficiency of cellular internalization was nonlinear, and the capacity of neurons to take up hsiRNA^{HTT}-loaded exosomes appeared saturable (**Figure 2c**). This finding is consistent with the kinetics of uptake observed with microscopy (**Figure 2a,b**).
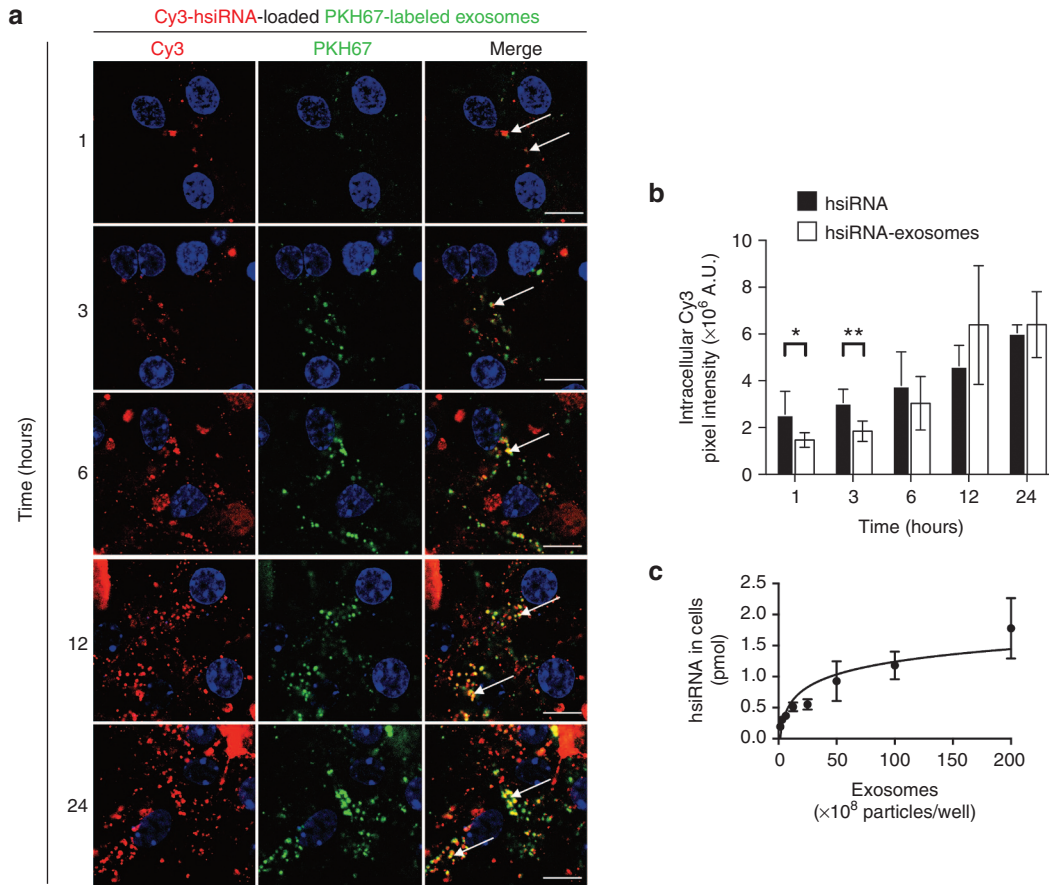
Figure 2 Internalization of hydrophobic Cy3-hsiRNA-loaded exosomes by primary cortical neurons. (a) Kinetics of Cy3-hsiRNA^{HTT}-loaded exosomes shows significant co-localization between exosomes and hsiRNAs. hsiRNA^{HTT} labeled with Cy3 (red); exosomes labeled with PKH67 (green); nuclei labeled with Hoechst (blue). Samples were visualized at 63× magnification. Scale bar = 10 μm. Arrows show hisRNA^{HTT}-exosomes. **(b)** Bar graphs showing the absolute quantification of Cy3-fluorescence in cells upon incubation with Cy3-hsiRNA (black) or Cy3-hsiRNA-exosomes (white) ($n = 5$; mean ± SD; *$P < 0.05$, **$P < 0.01$, paired t-test comparing the Cy3 intensity of hsiRNA nonloaded versus loaded in exosomes). **(c)** Quantification of Cy3-hsiRNA^{HTT} taken up by primary neurons with increasing amounts of Cy3-hsiRNA^{HTT}-loaded exosomes. The level of Cy3-labeled hsiRNAs was measured by high-performance liquid chromatography ($n = 3$ technical replicates; mean ± SD). hsiRNA, hydrophobically modified small interfering RNA.
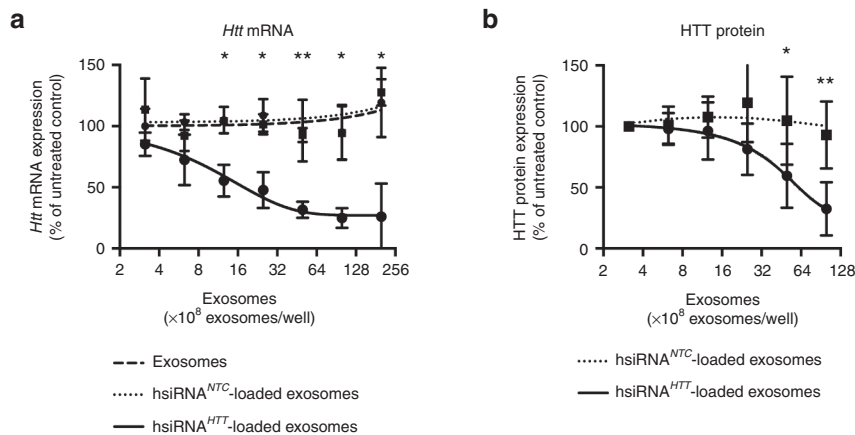

Figure 3 Concentration-dependent silencing of *Huntingtin* mRNA and protein by hsiRNA^{HTT}-loaded exosomes in primary cortical neurons. **(a)** Graph of *Htt* mRNA levels in cells treated with increasing amounts of hsiRNA^{HTT}-loaded exosomes (solid line), hsiRNA^{NTC}-loaded exosomes (dotted line), or nonloaded exosomes (dashed line) for 7 days. *Htt* mRNA levels are normalized to *Ppib* mRNA (housekeeping control) and presented as percent of untreated control ($n = 4$ biological replicates, each performed with $n = 3$ technical replicates; mean ± SD; *$P < 0.05$, **$P < 0.01$, paired t-test comparing each concentration to hsiRNA^{NTC}-loaded exosomes). **(b)** Graph of HTT protein levels in cells treated with increasing amounts of hsiRNA^{HTT}-loaded exosomes (solid line; $n = 5$ biological replicates) or hsiRNA^{NTC}-loaded exosomes (dotted line; $n = 3$ biological replicates) for 7 days. HTT signal was normalized to Tubulin. Data at each concentration are presented as percent of untreated control samples (mean ± SD; *$P < 0.05$, **$P < 0.01$, paired t-test comparing each concentration to untreated samples). hsiRNA, hydrophobically modified small interfering RNA; NTC, nontargeting control.

To assess whether exosome-mediated hsiRNA^{HTT} delivery productively silences *Htt* mRNA and protein, we treated mouse primary cortical neurons for 7 days with increasing doses of hsiRNA^{HTT}-loaded exosomes (**Figure 3**). As a negative control, cells were treated with exosomes loaded with nontargeting hsiRNA^{NTC}. We observed dose-dependent silencing of *Htt* mRNA (up to 75% reduction; **Figure 3a**) and HTT protein (up to 68% reduction; **Figure 3b** and **Supplementary Figure S5** for original Western blot). Neither hsiRNA^{HTT} alone nor hsiRNA^{HTT}-loaded exosomes affected the expression levels of housekeeping controls (*Ppib* mRNA and Tubulin protein; **Supplementary Figure S5**). We estimated that exosome-associated hsiRNA^{HTT} induced *Htt* mRNA silencing with a half-maximal inhibitory concentration (IC$_{50}$) in the low nanomolar range, which required treatment with at least 25×10^8 exosomes per well (**Figure 3a**). These results suggest that exosomes support efficient neuronal delivery and do not interfere with hsiRNA-RISC assembly or hsiRNA-mediated silencing.
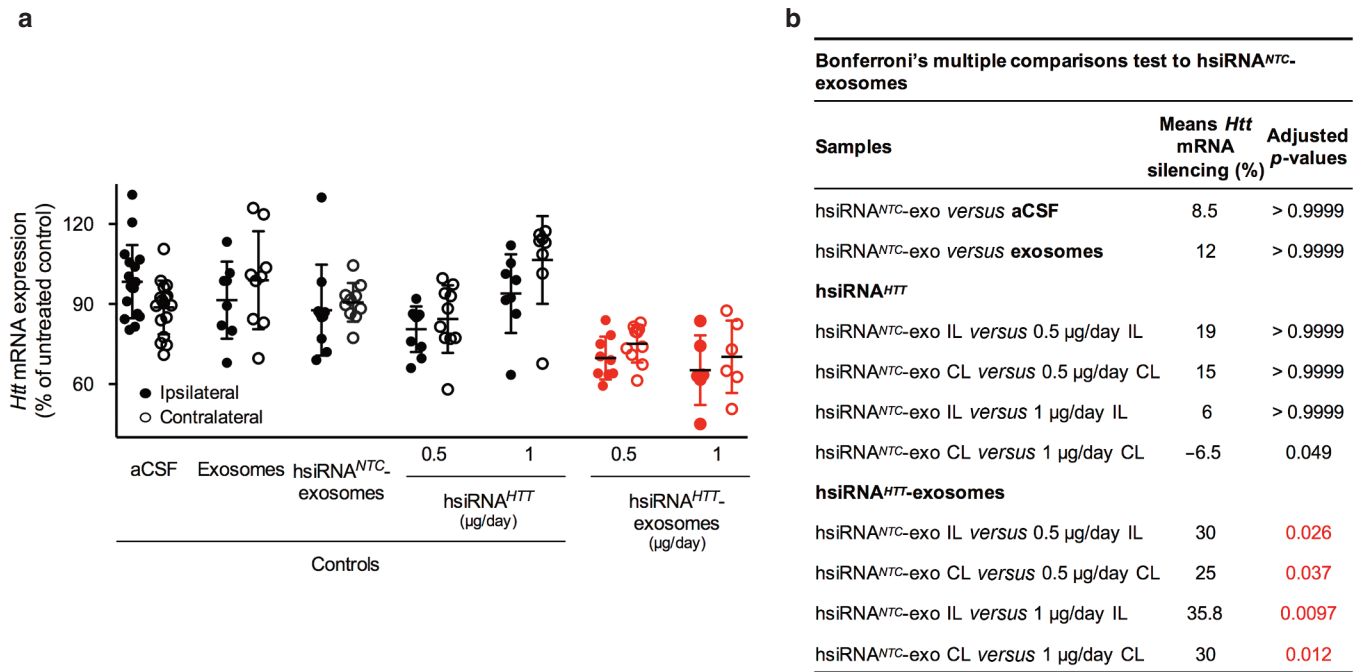
hsiRNA-loaded exosomes distribute bilaterally in the brain upon unilateral brain infusion

Saturable uptake of exosomes by neurons might be advantageous for *in vivo* delivery and promote wide distribution of oligonucleotides throughout the brain. To test this, we infused Cy3-hsiRNA^{HTT}-loaded exosomes directly into mouse striatum for 7 days (0.5 µg hsiRNA/day) and then examined the distribution of hsiRNAs throughout the brain. Unilateral delivery of Cy3-hsiRNA^{HTT}-loaded exosomes led to bilateral distribution of fluorescence throughout the brain, including the striatum and cortex (**Figure 4a**). We did not observe fluorescence in brains infused with unlabeled hsiRNA^{HTT}-loaded exosomes (**Figure 4b**), demonstrating that fluorescence is due to the Cy3-hsiRNA^{HTT} rather than an increase in tissue autofluorescence.

Structural damage at the infusion site was similar in all treated brains, including those treated with PBS. A high level of fluorescence appeared to accumulate around the infusion site. This
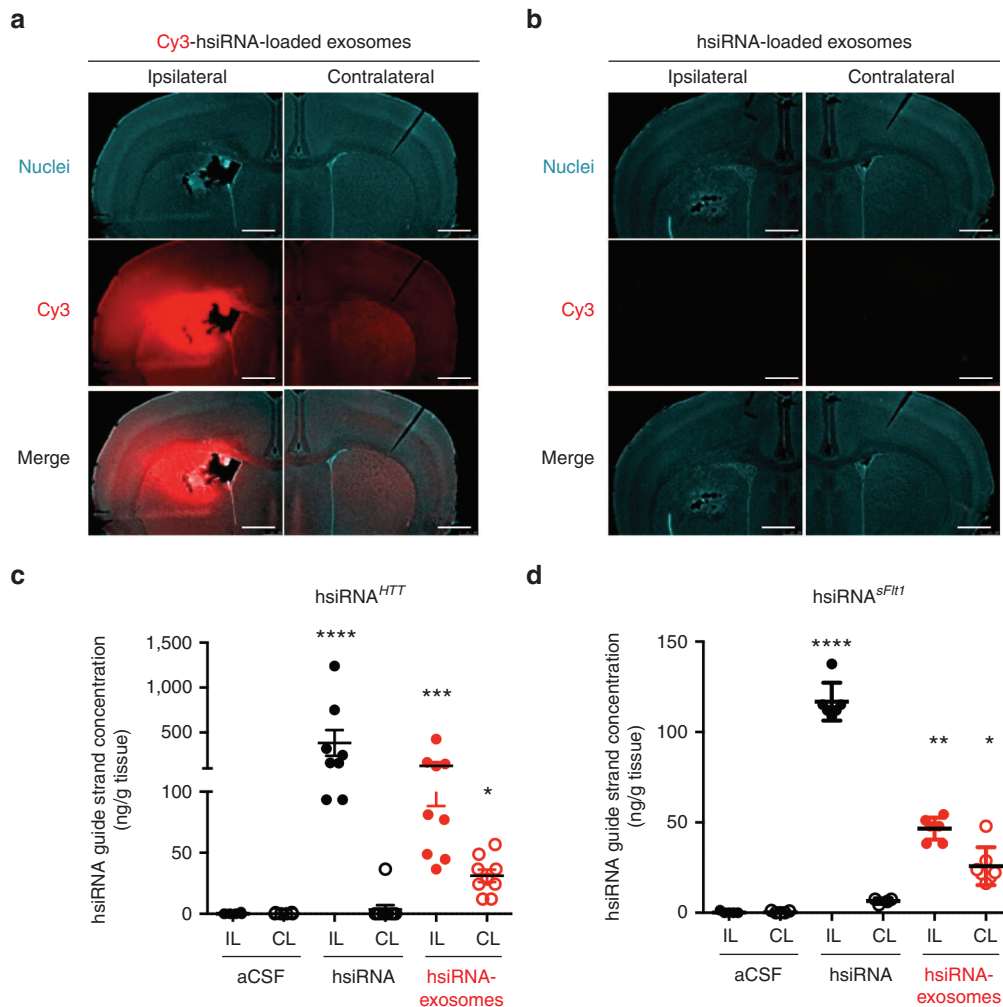
Figure 4 Exosomes promote bilateral distribution of hsiRNAs. (a,b) Images of ipsilateral (left) and contralateral (right) brain sections after infusion of Cy3-hsiRNA^{HTT}-loaded exosomes (red) (**a**) or unlabeled hsiRNA^{HTT}-loaded exosomes (**b**). Nuclei stained with Hoechst (blue). Samples were visualized at 2.5× magnification. Scale bar = 1 mm. All pictures were acquired with the same microscope settings. (**c,d**) Plot showing tissue concentrations of hsiRNA^{HTT} (**c**) or hsiRNA^{sFlt1} (**d**) guide strands measured by peptide nucleic acid hybridization in biopsies from the ipsilateral (IL) and contralateral (CL) striata of mice treated with hsiRNA-loaded exosomes, hsiRNAs alone, or artificial cerebrospinal fluid (CSF) (hsiRNA^{HTT}, *n* = 7 mice per group; hsiRNA^{sFlt1}, *n* = 9 mice per group). Each point in the plot represents the level of hsiRNA guide strands in an individual mouse, and the mean ± SD of each group is indicated. Data were analyzed using a nonparametric Kruskal–Wallis test, and the mean of each column was compared to the mean of the corresponding artificial CSF control column. *P < 0.05, **P < 0.01, ***P < 0.001, ****P < 0.0001. hsiRNA, hydrophobically modified small interfering RNA.

a

b

Bonferroni's multiple comparisons test to hsiRNA^{NTC}-exosomes		
Samples	**Means Htt mRNA silencing (%)**	**Adjusted p-values**
hsiRNA^{NTC}-exo *versus* **aCSF**	8.5	> 0.9999
hsiRNA^{NTC}-exo *versus* **exosomes**	12	> 0.9999
hsiRNA^{HTT}		
hsiRNA^{NTC}-exo IL *versus* 0.5 µg/day IL	19	> 0.9999
hsiRNA^{NTC}-exo CL *versus* 0.5 µg/day CL	15	> 0.9999
hsiRNA^{NTC}-exo IL *versus* 1 µg/day IL	6	> 0.9999
hsiRNA^{NTC}-exo CL *versus* 1 µg/day CL	–6.5	0.049
hsiRNA^{HTT}-exosomes		
hsiRNA^{NTC}-exo IL *versus* 0.5 µg/day IL	30	0.026
hsiRNA^{NTC}-exo CL *versus* 0.5 µg/day CL	25	0.037
hsiRNA^{NTC}-exo IL *versus* 1 µg/day IL	35.8	0.0097
hsiRNA^{NTC}-exo CL *versus* 1 µg/day CL	30	0.012

Figure 5 hsiRNA^{HTT}-loaded exosomes induce bilateral Htt mRNA silencing *in vivo* in mouse brain. (a) Plots showing Htt mRNA levels in biopsies from the ipsilateral (closed) and contralateral (open) striata of mice treated with artificial cerebrospinal fluid (CSF), unloaded exosomes, hsiRNA^{NTC}-loaded exosomes, 0.5 and 1 µg/day hsiRNA^{HTT}, or 0.5 and 1 µg/day hsiRNA^{HTT}-loaded exosomes (red). Exosomes were delivered at 2–4 × 10^{10} particles/day. Level of Htt mRNA was normalized to $Ppib$ mRNA (housekeeping control), and data are presented as percent of untreated control (n = 6–10 mice per group). Each point represents the averaged level of Htt mRNA from three biopsies of an individual mouse, and the mean ± SD of each group is indicated. **(b)** Bonferroni's multiple comparison tests between groups treated with artificial CSF, exosomes, hsiRNA^{HTT}, or hsiRNA^{HTT}-exosomes and group treated with hsiRNA^{NTC}-loaded exosomes. IL, ipsilateral; CL, contralateral; hsiRNA, hydrophobically modified small interfering RNA; NTC, nontargeting control.

local accumulation might result in part from direct exposure to exosomes or exosomal degradation and local release of Cy3-hsiRNAs. A single unilateral injection of Cy3-hsiRNA alone (*i.e.*, not loaded into exosomes) also resulted in a local accumulation of fluorescence proximal to the injection site but fluorescence was not detected contralateral to the injection site.[14] Thus, exosomes deliver hsiRNAs to both sides of the brain after unilateral administration.

To quantitatively confirm the observed exosome-dependent bilateral hsiRNA distribution, we used a PNA-based hybridization assay. This assay directly quantifies the levels of hsiRNA guide strand tissue accumulation[34] (**Figure 4c,d**). A week after infusion, we harvested striata from mice infused with hsiRNA^{HTT}-loaded exosomes, hsiRNA^{HTT} alone (nonloaded), or artificial CSF (aCSF) (control). Nonloaded hsiRNAs accumulated in the ipsilateral striata, but not in the contralateral striata. The guide strand of hsiRNA^{HTT} delivered by exosomes was detected in both ipsilateral and contralateral striata, consistent with bilateral fluorescence of Cy3-labeled guide strand detected *in situ* (**Figure 4c**). We obtained similar results using a different hsiRNA, hsiRNA^{sFlt1}, targeting the *sFlt-1* mRNA (**Figure 4d**). Together these data suggest that local infusion of hsiRNA-loaded exosomes supports widespread delivery of hsiRNAs throughout the brain.

hsiRNA^{HTT}-loaded exosomes induce bilateral Htt mRNA silencing *in vivo*

To determine whether the bilateral distribution of hsiRNA^{HTT} results in widespread Htt mRNA silencing, we infused

hsiRNA^{HTT}-loaded exosomes (0.5 or 1 µg/day) into the striata of wild-type mice for 7 days (**Figure 5**). As controls, we infused aCSF, unloaded exosomes, hsiRNA^{NTC}-loaded exosomes (nontargeting control), or nonformulated hsiRNA^{HTT} (0.5 and 1 µg/day). At the end of the treatment, we measured Htt mRNA levels in ipsilateral and contralateral striata and compared to aCSF-treated or hsiRNA^{NTC}-loaded exosomes samples (**Figure 5**, **Supplementary Table S1**). Treatment with hsiRNA^{HTT}-loaded exosomes resulted in statistically significant bilateral reduction of Htt mRNA at both concentrations used (**Figure 5**, **Supplementary Table S1**). Bilateral silencing triggered by hsiRNA^{HTT}-loaded exosomes is consistent with the bilateral distribution of fluorescent hsiRNA-loaded exosomes described above (**Figure 4**). At the doses tested, hsiRNA^{HTT} did not reduce Htt mRNA levels—not even ipsilateral to the injection site—indicating that exosomes are essential for hsiRNAs distribution and function throughout the brain (**Figure 5**). Silencing induced by hsiRNA^{HTT}-loaded exosomes was similarly significant when compared to aCSF-treated animals (**Supplementary Table S1**). These findings demonstrate that the exosome-mediated bilateral hsiRNA distribution was functionally significant.

hsiRNA-loaded exosomes do not induce measurable cytotoxicity or innate immune activation

A viable delivery vehicle should have minimal innate immunostimulation and cytotoxicity. We measured the levels of microglia activation and cell death after administering exosomes to the brain (**Supplementary Figures S6–S8**). Microglia and monocytes

are activated by brain injury and can be identified by Iba1 staining, a marker of neuroinflammation.[35] Activated microglia show increased Iba1 staining, enlarged cell bodies, and ramified processes. Because some of the innate immune response may be transient and disappear by 7 days postinjection, we evaluated the microglia response at 6 hours after injection of hsiRNA^{HTT}-loaded exosomes (**Supplementary Figure S6**). The histopathology and morphology of microglia staining were comparable between mice injected with PBS, exosomes alone, or hsiRNA^{HTT}-loaded exosomes (**Supplementary Figure S6**). Visual evaluation of treated and untreated brains did not show any inflammatory events (**Supplementary Figure S6a,b**). Intracranial injection with PBS caused a marginal activation of microglia in the ipsilateral side of the brain, mostly related to needle-induced trauma. The number of activated microglia was increased by exosomes alone but not by hsiRNA^{HTT}-loaded exosomes, suggesting a minor neuroinflammation enhanced by exosomes only (**Supplementary Figure S6c**). This effect was minor and fully resolved by 7 days (**Supplementary Figure S7**).

To assess the impact of exosome-mediated delivery of oligonucleotides on neuronal integrity, we stained for the dopamine receptor DARPP32, a marker for neuronal viability expressed on medium spiny neurons in the striatum (**Supplementary Figure S8**). The histopathology and quantification of DARPP32-positive cells was comparable between mice infused with PBS, exosomes alone, or hsiRNA^{HTT}-loaded exosomes (**Supplementary Figure S8**); we did not observe any negative impact on DARPP32 staining in all samples.

DISCUSSION

The discovery that extracellular vesicles mediate the transport of functional small RNAs between cells has raised considerable interest for exosomes to serve as a novel delivery vehicle for therapeutic oligonucleotides.[36] Methods of loading oligonucleotides into exosomes have included electroporation[29,37] or overexpression of siRNA in exosome-producing cells.[38–40] Though useful for proof-of-principle experiments, neither method can be easily controlled or scaled for production.[41] Moreover, electroporation was shown to disrupt exosome integrity,[41] thereby dampening enthusiasm for the potential utility of exosomes for therapeutic oligonucleotide delivery.

We have shown that co-incubating hsiRNAs with exosomes provides a robust, efficient, and highly reproducible method for loading exosomes with chemically synthesized oligonucleotides. We believe that this methodology could easily be used to load other classes of therapeutic oligonucleotides, including micro-RNAs, antisense oligonucleotides, antagomirs, or aptamers, as long as the oligonucleotides are stable and hydrophobically modified. The simplicity of this method should accelerate research into the use of exosomes for delivery of ONTs.

The hsiRNA-loaded exosomes are stable during the preparation and the loading of the vesicles with the oligonucleotides did not interfere with their physical (size, appearance) or functional (trafficking, brain distribution) properties (**Figures 1** and **2**). Efficient loading requires extensive chemical stabilization of siRNAs. Indeed hsiRNAs have >60% of ribose's chemically modified with 2′-O-methyl and 2′-fluoro modifications resulting in

significant resistance to nuclease degradation.[12] With increase in the hsiRNA/vesicle loading ratio, we have seen a slight increase in surface negative charge indicating that hsiRNAs associate with vesicle membrane. This is consistent with electron microscopy that confirmed presence of oligonucleotides on the surface and in the lumen of exosomes; hsiRNA-loaded exosomes are stable and externally bound hsiRNAs are resistant to nucleases. At this point, we cannot define which of the exosomes-associated oligonucleotides (surface bound or internalized) are functionally active. The amount of hsiRNA associated with exosomes is affected by hsiRNA/exosomes ratio during the loading procedure. The loading is saturable and a maximum of ~3,000 hsiRNA can be loaded per individual vesicle. Too much loading might interfere with native exosome-uptake mechanism as the loading of hsiRNAs does influence the surface charge of exosomes. Further studies are essential to determine the optimal loading, long-term stability, and *in vivo* behavior of the hsiRNA-loaded exosomes.

What is the mechanism of exosomes driven bilateral brain distribution? Retrograde transport of hsiRNA^{HTT}-loaded exosomes along nerve fiber tracts could account for the presence of hsiRNA^{HTT} in cortical layers on both sides of the brain, and anterograde transport could promote the spread of hsiRNA^{HTT} to the contralateral striatum.[42] Although significantly more fluorescence accumulated ipsilateral to the infusion site than contralateral, the level of intact guide strand, detected using PNA hybridization assay[34] (**Figure 4c,d**), and *Htt* mRNA silencing (**Figure 5**) were generally similar on both sides of the brain. The excess of fluorescence around the injection site likely reflects local accumulation of the Cy3-hsiRNA^{HTT} degradation products, as levels of full-length guide strands were similar. Further enhancement of hsiRNA stability should allow development of loading in vesicles with better distribution and efficacy.

The contralateral distribution of hsiRNAs is dependent on their loading in exosomes. Infusion of equal amounts of nonloaded hsiRNAs did not result in detectable transfer of oligonucleotides to the noninjected side of the brain. Most of the nonloaded hsiRNAs stayed at the injected side of the brain and relatively high levels are easily detectable by the PNA hybridization assay (**Figure 4**). Intact oligonucleotides were detectable, but were functionally inactive at the same dose (**Figure 5**). This might be related to preferentially binding of cholesterol-modified oligonucleotides to hydrophobic myelinated fibers, limiting neuronal access. In bolus injection, a large amount of oligonucleotides is delivered simultaneously saturating the tissue matrix, with excess of the oligonucleotides available for functional neuronal trafficking. Similar trends were observed with antisense oligonucleotides, where bolus injection supported better efficacy and functional tissue accumulation than slow, continuous infusion with the pumps.[14] In the ipsilateral side of the brains, hsiRNAs loaded in exosomes accumulated to the similar or even lower levels than nonloaded oligonucleotides. The level of accumulation was lower, but sufficient to support *Htt* mRNA silencing. This indicates that hsiRNAs loaded in exosomes traffic differently from unloaded hsiRNAs *in vivo*.

Our hope is that exosome-mediated delivery of oligonucleotides can reduce the effective concentration of oligonucleotide required for silencing in the brain. In a recent study, infusion of 700 µg of antisense oligonucleotide was required to efficiently

silence *Htt* mRNA.[5] We have shown here that infusion of as little as 3.5–7 μg of hsiRNA*HTT* over 1 week (1 μg/day) is sufficient to reduce *Htt* mRNA levels by ~35%, but only when hsiRNAs are loaded in exosomes. Our findings therefore suggest that exosomes increase hsiRNA stability, promote *in vivo* bilateral spreading of hsiRNAs, and enter a potent neuronal uptake pathway. The bilateral efficacy was consistent with exosome-mediated distribution of mature guide strands to both sides of the brain as detected by PNA hybridization assay (**Figure 4b**).

We only observed partial modulation of *Htt* mRNA expression (~35%) on both sides of the brain. While moderate, the silencing was highly statistically significant when compared to aCSF and exosomes formulated with nontargeting control (NTC). Further optimization of hsiRNA stability, loading, and exploration of different exosome sources will likely increase the efficiency of silencing. Partial *Htt* mRNA silencing (40–50%) *in vivo* was previously demonstrated to be sufficient to prevent or delay disease phenotypes, neuropathology, and behavior abnormalities in several mouse models of HD.[4–6] Clinically, it is likely that only partial *HTT* mRNA silencing will be optimal as complete gene elimination could be detrimental long-term.[43,44]

Translation of exosome-based therapeutics to the clinic will require identification of cell types, culture conditions, and purification methods that allow large-scale production of exosomes with minimal immunogenicity. Here, we used exosomes derived from the human U87 glioblastoma cell line. U87 cells produce a high level of exosomes and U87-derived exosomes are efficiently loaded with hsiRNA and show trafficking abilities into neurons.

We used human-derived exosomes in mouse and did not observe any significant increase in neuroinflammation levels over levels induced by infusion (aCSF versus hsiRNA-loaded exosomes, **Supplementary Figures S6 and S7**). There was minor, reversible increase in numbers of activated microglia (**Supplementary Figure S6**) at the injection side of animals treated with exosomes (not loaded with hsiRNAs). hsiRNA-loaded exosomes did not show the same effect. Interestingly, heavily modified oligonucleotides have been shown to dampen immune response.[45]

We recognize that use of tumor-derived exosomes might raise concerns for clinical applications. There are multiple publications indicating roles of tumor-derived exosomes in cancer pathogenesis.[46] We are currently screening different clinically acceptable cell sources, including mesenchymal stem cells, to produce exosomes. Thus, a next challenge is optimizing the production of exosomes of high quality and purity from other cell sources (examples include stem cells and dendritic cells). A better understanding of exosome components responsible for neuronal uptake could lead to engineered vesicles with similar properties. Neural stem cells or exosomes derived from stem cells are being considered as a therapeutic modality for the treatment of stroke[47,48] or neurodegenerative disorders.[37,49] The data presented here allow additional loading of exosomes with chemically synthesized therapeutic siRNAs or microRNAs.

In conclusion, here we describe a novel method for efficient loading of oligonucleotide cargo onto exosomes and the ability of exosomes to deliver cargo *in vitro* in primary neurons and *in vivo* in mouse brain. The ability of this "natural" oligonucleotide delivery strategy to promote the distribution and improve the efficacy of oligonucleotides represents an important step toward development of novel therapies for HD and other neurodegenerative disorders.

MATERIALS AND METHODS

Oligonucleotides. Oligonucleotide sequences and chemical modification patterns used in this study are described in **Table 1**.

Cell culture. U87 glioblastoma cells were maintained in Dulbecco's modified essential medium (DMEM) (Cellgro, Corning, NY; #10-013CV) supplemented with 100 U/ml penicillin-streptomycin (Invitrogen, Carlsbad, CA; #15140) and 10% fetal bovine serum (Gibco, Carlsbad, CA; #26140) at 37 °C, 5% CO_2, and 100% humidity. For the production of exosomes, glioblastoma cells were cultured in exosome-free medium prepared with DMEM supplemented with 400 U/ml penicillin-streptomycin and 40% fetal bovine serum, and ultracentrifuged in 70 ml polycarbonate bottles (Beckman Coulter, Brea, CA; #355622) overnight at 100,000*g*, 4 °C using a Type 45 Ti rotor (Beckman Coulter; #339160). The supernatant, corresponding to 4× culture medium, was filtered in 0.2 μm filter bottle and diluted with DMEM to obtain 1× medium.[50]

Preparation of primary cortical neurons. Primary cortical neurons were isolated from E15.5 mouse embryos of wild-type FVBNj mice. Pregnant females were anesthetized by intraperitoneal injection of Avertin at 250 mg/kg body weight (Sigma, St. Louis, MO; #T48402) followed by cervical dislocation. Embryos were removed and transferred to ice-cold DMEM/F12 medium (Invitrogen; #11320). Brains were removed and meninges were carefully detached. Cortices were isolated and transferred into prewarmed papain solution for 25 minutes at 37 °C, 5% CO_2 to dissolve the tissue. Papain (Worthington, Lakewood, NJ; #54N15251) was dissolved in 2 ml Hibernate E (Brainbits, Springfield, IL; #HE) and 1 ml EBSS (Worthington; #LK003188) and supplemented with 0.25 ml of 10 mg/ml DNase1 (Worthington; #54M15168) in Hibernate E. After the 25-minute incubation, the papain solution was removed and 1 ml NbActiv4 (Brainbits; #Nb4-500) supplemented with 2.5% fetal bovine serum was added to the tissue. Tissues were then dissociated by trituration through a fire-polished, glass Pasteur pipet. Neurons were counted and diluted at 1×10^6 cells/ml. For live-cell imaging studies, 2×10^5 cells were plated in glass-bottom dishes (MatTek, Ashland, MA; #P35G-1.5-10-C) precoated with poly-L-lysine (Sigma; #P4707). For *in vitro* silencing assays, 1×10^5 neurons per well were plated on 96-well plates precoated with poly-L-lysine (BD BIOCOAT, Corning, NY; #356515). After overnight incubation at 37 °C, 5% CO2, an equal volume of NbActiv4 supplemented with anti-mitotics, 0.484 μl/ml of 5′UtP (Sigma, St Louis, MO; #U6625) and 0.2402 μl/ml of 5′FdU (Sigma, St Louis, MO; #F3503) was added to neuronal cultures to prevent the growth of non-neuronal cells. Half of the volume of media was replaced with fresh NbActiv4 containing anti-mitotics every 48 hours until the experiments were performed.

Purification and characterization of exosomes. Exosomes were purified from U87 glioblastoma cells as described[33,51] (**Supplementary Figure S1A**). Conditioned culture medium containing exosomes was harvested and centrifuged at 300*g* for 10 minutes. The supernatant was then centrifuged at 10,000*g*, 4 °C for 30 minutes and filtered in a 0.2 μm filter bottle. The filtered medium was centrifuged in 70 ml polycarbonate bottles for at least 70 minutes at 100,000*g*, 4 °C using a Type 45 Ti rotor (Beckman Coulter). Pellets were suspended in 1 ml PBS and centrifuged for 1 hour at 100,000*g*, 4 °C in a tabletop ultracentrifuge using a TLA-110 rotor (Beckman Coulter; #366730). Pellets were suspended in PBS for further experiments. For each sample, the concentration and size of particles were determined by recording and analyzing the Brownian motion of particles using a NanoSight NS300 system and Nanoparticles Tracking Analysis software (Malvern, Worcestershire, United Kingdom) according to the manufacturer's protocol. Samples were diluted in 1 ml PBS at room temperature and monitored in duplicate for 30 seconds with manual

shutter and gain adjustments. The recorded videos were analyzed using a Nanoparticle Tracking Analysis software. Particle charges were determined by diluting sample in 1 ml water and measuring the zeta potential in the universal glass cuvette Dip Cell kit (Malvern; #ZEN1002) using a Zetasizer Nano NS (Malvern).

Loading of exosomes with hsiRNAs and fluorescent labeling. Exosomes were loaded with indicated concentration of Cy3-fluorescent hsiRNAs in PBS by incubation at 37 °C for 90 minutes with shaking at 500 rpm. Unloaded hsiRNAs were separated from hsiRNA-loaded exosomes by ultracentrifugation for 1 hour at 100,000*g*, 4 °C in a tabletop ultracentrifuge using a TLA-110 rotor (**Figure 1**). Unloaded hsiRNAs remain in the supernatant and hsiRNA-loaded exosomes form a pellet (**Supplementary Figure S2b**). Pellets were suspended in PBS for *in vitro* uptake experiments or in cell medium for *in vitro* silencing analysis. The Cy3 fluorescence of the supernatant (containing unloaded hsiRNA) and the pellet (containing hsiRNA-exosomes) was measured in a Costar UV-transparent, flat-bottom 96-well plate (Corning; #3635) using an Infinite M1000 Pro spectrophotometer (Tecan, Männedorf, Switzerland; 547 nm excitation and 570 nm emission wavelengths), using a calibration curve for the quantification. The loading efficiency of hsiRNAs in exosomes was estimated by two methods. First, by directly measuring the Cy3 fluorescence in the hsiRNA-exosomes pellet. Second, by calculating the difference between the total amount of Cy3-hsiRNA originally added to the sample and the amount of Cy3-hsiRNA remaining in the supernatant after exosome incubation and ultracentrifugation.

The exosomes concentration was measured by Nanoparticle Tracking Analysis using a Nanosight (Malvern). The number of hsiRNAs loaded per exosomes was estimated by dividing the total amount of hsiRNAs in the sample by the number of exosomes detected by Nanoparticle Tracking Analysis, assuming normal distribution. The experimental input was always normalized by the amount of hsiRNA added (loaded or not), with level of hsiRNA loading being similar between different exosomes preparations.

Animal stereotaxic injections. All animal procedures were approved by the University of Massachusetts Medical School Institutional Animal Care and Use Committee (protocol number A-2411). Prior to oligonucleotide injection, animals were deeply anesthetized with 1.2% Avertin (Sigma; #T48402). For direct injection, wild-type FVBNj mice received microinjections by stereotactic placement into the right striata (coordinates relative to bregma were 1.0 mm anterior, 2.0 mm lateral, and 3.0 mm ventral). For brain infusion, ALZET osmotic pumps (ALZET, Cupertino, CA; #1007D) were prefilled with 100 µl of sample following manufacturer instructions and primed overnight at 37 °C in a water bath. Oligonucleotide was delivered at a flow rate of 0.5 µl/hour for 7 days.

For *in vivo* silencing of *Htt* mRNA, mice were treated with aCSF (100 µl per pump, *n* = 9 mice), 20–30 × 10⁹ particles/day of exosomes alone (100 µl per pump, *n* = 9 mice), 1 µg/day of NTC siRNA associated with 20–30 × 10⁹ particles/day of exosomes (100 µl per pump, *n* = 10 mice), 0.5 or 1 µg/day hsiRNA^{HTT} alone (100 µl per pump, *n* = 10 mice and *n* = 8 mice per group, respectively), and 0.5 or 1 µg/day of hsiRNA^{HTT} associated with 20–30 × 10⁹ particles/day of exosomes (100 µl per pump, *n* = 9 mice and *n* = 6 mice per group, respectively). Upon 7 days of treatment, mice were killed and brains were harvested and processed as described below.

For analysis of immunoreactive DARPP32 and Iba1 neurons, mice received injections or pump infusion (100 µl) of either PBS or aCSF (2 µl per striata, or 100 µl per pump, *n* = 5 mice), 20–30 × 10⁹ particles/day of exosomes alone (2 µl per striata, or 100 µl per pump, *n* = 5 mice), or of hsiRNA^{HTT}-exosomes (2 µl per striata or 100 µl per pump, *n* = 5 mice). Mice were killed 6 hours or 7 days later.

mRNA quantification. The mRNA levels were quantified using the QuantiGene 2.0 Assay (Affymetrix, Santa Clara, CA; #QS0011).

For *in vitro* experiments, cells were plated at 1 × 10⁵ neurons per well in 96-well plate and lysed in 250 µl diluted lysis mixture per well

(Affymetrix; #13228) supplemented with 0.167 µg/µl proteinase K (Affymetrix; #QS0103) for 30 minutes at 55 °C. Cell lysates were mixed thoroughly and 40 µl (~16,000 cells) of lysate was added to the capture plate along with 40 µl additional diluted lysis mixture without proteinase K. Probe sets were diluted as specified in the Affymetrix protocol. Twenty microliters of mouse *Htt* or *Ppib* probe sets (Affymetrix; #SB-14150, #SB-10002) was added for a final volume of 100 µl per sample well.

For *in vivo* experiments, brains were harvested and sliced from the front into 300 µm coronal sections using a Leica Vibratome 2000T (Leica Biosystems, Wetzlar, Germany). The fourth section from the front corresponds to the beginning of the striatum. The next three consecutive coronal sections (fifth, sixth, and seventh sections) were selected to collect one 2 mm biopsy from the striatum of each hemisphere of each section (*i.e.*, three biopsies per animal per hemisphere) using a sterile disposable biopsy punch with plunger (Miltex, York, PA; #33-31-P) and placed in RNAlater (Ambion, Carlsbad, CA; #AM7020) for 24 hours at 4 °C. The position of the biopsy is strictly fixed and samples were always collected from the same region of the brain for all animals. All samples were stored in RNAlater at −80 °C until further analysis. Tissue biopsies were lysed in 300 µl homogenizing buffer (Affymetrix; #10642), supplemented with 2 µg/µl proteinase K per 5 mg tissue punch, and homogenized in 96-well plate format on a TissueLyser II (Qiagen, Hilden, Germany). Forty microliters each lysate was added to the capture plate and mixed with 60 µl of diluted *Htt* or *Ppib* probe sets for a final volume of 100 µl. Signal was amplified according to the Affymetrix QuantiGene protocol. Luminescence was detected on a Veritas Luminometer (Promega, Madison, WI). The average of the three biological replicates (three biospsies) represents the mRNA expression value per animal.

Protein level quantification. Primary cortical neurons were plated at 1 × 10⁵ neurons per well in 96-well plates and treated as described in **Figure 3**. Upon 7 days treatment, cells were lysed in 20 µl lysis buffer (50 mmol/l Tris pH 7.4, 250 mmol/l NaCl, 1% NP40, 5 mmol/l ETDA) supplemented with protease inhibitors (1 tablet per 10 ml buffer; Roche, Basel, Switzerland; #11836170001). Plates were incubated 15 minutes on ice, with shaking. Cell lysates from technical triplicates were pooled and stored at −80 °C until Western blots were performed. Lysates (20 µg) were boiled, then proteins were separated on Novex NuPage 3–8% Tris-Acetate gels (Life Technologies, Carlsbad, CA; #EA03755) and transferred to nitrocellulose using a TransBlot Turbo apparatus (BioRad, Hercules, CA; #1704155). Nitrocellulose membranes were blocked in 5% blotting grade blocker (BioRad; #1706404) in Tris-buffered saline, 0.1% Tween-20 (TBST) for 1 hour at room temperature and then incubated overnight in primary antibody diluted in blocking solution. The blots were cut horizontally, and the top of each blot was incubated with rabbit polyclonal anti-HTT antibody Ab1 (ref. 52) (1:2,000 in blocking buffer), while the bottom of each blot was incubated with mouse monoclonal anti-tubulin antibody (1:6,000 in blocking buffer; Sigma) as a loading control. Blots were washed in TBST and then incubated with either peroxidase-labeled anti-rabbit IgG diluted (1:2,500 in blocking buffer) or anti-mouse IgG diluted (1:5,000 in blocking buffer) for 1 hour at room temperature. Blots were washed in TBST, and bands illuminated using SuperSignal West Pico Chemiluminescent Substrate (Thermo Scientific, Carlsbad, CA; #34080) were captured on X-ray film. Images were scanned using an Epson Perfection V750 Pro (Epson, Tokyo, Japan), and densitometry was performed on manually identified bands using ImageJ software (NIH, Bethesda, MA).

PNA hybridization assay. hsiRNA guide strands in tissue lysates were quantified using a PNA hybridization assay (developed by Axolabs GmbH, Kulmbach, Germany).[34] PNAs are analogues of DNA in which the sugar-phosphate backbone is replaced with a polyamide backbone. Tissues were lysed in MasterPure Tissue Lysis Solution (EpiCentre, Madison, WI; #MTC096H) supplemented with 2 mg/ml proteinase K (Invitrogen; #25530-049) on a TissueLyser II (10 mg tissue in 100 µl lysis solution). Sodium dodecyl sulfate was precipitated with 3 mol/l KCl and pelleted at

5,000g. hsiRNA guide strands in cleared supernatant were hybridized to fully complementary Cy3-labeled PNA strands (PNABio, Thousand Oaks, CA). The PNA sequence and chemical modification pattern used in this study are described in **Table 1**. hsiRNA-PNA duplexes were injected into HPLC DNAPac PA100 anion exchange column (Thermo Scientific), and Cy3 fluorescence was monitored and peaks integrated. The mobile phase for HPLC was 50% water, 50% acetonitrile, 25 mmol/l Tris-HCl (pH 8.5), 1 mmol/l ethylenediaminetetraacetate, and the salt gradient was 0–800 mmol/l $NaClO_4$. For the calibration curve, a known amount of hsiRNA duplex was spiked into tissue lysis solution.

Live cell staining. To monitor live-cell uptake of exosomes *in vitro*, exosomes or Cy3-labeled hsiRNA-loaded exosomes were fluorescently labeled with PKH67 dye (Sigma; #PKH67GL-1KT) by adding 10 µmol/l of PKH67 to the samples in 100 µl PBS, and incubated for 30 minutes at 37 °C. Free dye was washed from labeled exosomes using MV3000 Exosome Spin Column (Life Technologies; #4484449) according to the manufacturer's protocol. Primary neurons were plated at a density of 2×10^5 cells per 35-mm glass-bottom dish (MatTek; #P35G-1.5-10-C) precoated with poly-L-lysine (Sigma; #P4707). Nuclei were stained using the NucBlue Live ReadyProbe (Life Technologies; #R37605) according to the manufacturer's recommendation. Imaging was performed in 1 ml phenol red-free Hibernate E (Brainbits; #HE-Pr). Cells were treated with 0.2 µmol/l Cy3-labeled hsiRNA loaded in exosomes, 0.2 µmol/l Cy3-labeled hsiRNA alone, or exosomes, and live cell imaging was performed over time.

Immunohistochemistry of brain sections. *In vivo* cytotoxicity and microglia activation were monitored staining for immunoreactive DARPP32 and Iba1 proteins. Mice were perfused with PBS followed by paraformaldehyde, and brains were collected and randomized for single-blind processing and analysis. Brains were sliced into 40-µm sections in ice-cold PBS through the striatum using a Leica Vibratome 2000T (Leica Biosystems) (ref. Allen Brain Atlas). Immunohistochemistry was performed on every sixth section at room temperature unless stated.

For Iba1, sections were blocked with 5% normal goat serum and 1% bovine serum albumin in 0.2% Triton-X-100 and 0.03% hydrogen peroxide in PBS for 1 hour, washed with PBS, and incubated with anti-Iba1 (1:1,000 in blocking solution; Wako, Osaka, Japan; #019-19741) overnight at 4 °C. Sections were washed with PBS and incubated in biotinylated goat anti-rabbit secondary antibody (Vector Laboratories, Burlingame, CA) in PBS (1:200 dilution) for 10 minutes. After washing with PBS, biotinylated secondary antibody was labeled with peroxidase using the Vectastain ABC Kit (Vector Laboratories). Sections were washed with PBS, and peroxidase was visualized with 3,3′-diaminobenzidine (DAB) using the Metal Enhanced DAB Substrate Kit (Pierce, Rockford, IL).

For DARPP32 immunohistochemistry, sections were washed for 3 minutes in 3% hydrogen peroxide, and 20 minutes in 0.2% TritonX-100, and then blocked for 4 hours in PBS containing 1.5% normal goat serum. Sections were incubated with DARPP32 antibody (Abcam, Cambridge, United Kingdom; #40801) in 1.5% normal goat serum (1:10,000 dilution) at 4 °C overnight. Washes, binding of secondary anti-rabbit antibody, and labeling and detection of peroxidase were performed as described above.

Stained sections were mounted and visualized using a Nikon Eclipse E600 microscope under a 20× objective and imaged using a Nikon Digital Sight DSRi1 camera (Nikon, Tokyo, Japan). Four images were taken of ipsilateral and contralateral striata in each section. The number of DARPP32-positive neurons and Iba1-positive microglia was quantified using ImageJ (NIH). Full-brain coronal section scans were acquired with a Coolscan V-ED LS50 35mm Film Scanner (Nikon).

Confocal imaging. For the analysis of hsiRNA uptake *in vitro*, images were acquired with a Leica DM IRE2 confocal microscope using a 63× oil-immersion objective. Images were processed using ImageJ (1.47v) software (NIH). The relative uptake of hsiRNA, loaded or not in exosomes, was estimated based on pixel-integrated density of five images for each condition.

The percentage of colocalization was calculated based on Manders Overlap Coefficient using the Manders Coefficients plugin in ImageJ.

Size exclusion chromatography. Exosomes from U87 supernatants were purified as described above. Fifty microliters of cell-conditioned medium or 50 µl of exosomes was injected onto BioSep SEC-s4000 column (size exclusion column, pore size 500 Å) (Phenomenex, Torrance, CA) on an Agilent 1100 HPLC system (Agilent, Santa Clara, CA). Chromatography was conducted with 0.75 ml/minute flow rate with PBS as mobile phase. Eluted fractions were monitored at 220 nm using an Agilent DAD G1315B absorbance detector (Agilent).

Anion exchange chromatography. Primary cortical neurons were plated at 1×10^5 cells/well in a 96-well plate and treated with Cy3-labeled hsiRNA alone or with Cy3-labeled hsiRNA-loaded exosomes. After 4 days of incubation, media were transferred to a new 96-well plate, and the cells were lysed in Cell and Tissue Lysis Solution (EpiCentre; #MTC096H) containing proteinase K (Invitrogen; #25530-049). Sodium dodecyl sulfate from the lysis buffer was precipitated by 3 mol/l KCl and pelleted at 5,000g. Supernatant was injected onto a Dionex DNAPac P100 anion exchange column. Chromatography was performed using an Agilent 1100 HPLC system at 1 ml/minute flow rate in 50% water, 50% acetonitrile, 25 mmol/l Tris-HCl, pH 8.8, 1 mmol/l ethylenediaminetetraacetate, and salt gradient from 80 to 800 mmol/l $NaClO_4$. Cy3 fluorescence was detected in eluted fractions using an Agilent FLD1260 G1321B detector (Agilent).

Electron microscopy. Samples and grids for electron microscopy were prepared at room temperature unless otherwise specified. An equal volume of 4% paraformaldehyde was added to the exosome sample and incubated for 2 hours. Aliquots of exosomes (3 µl) were dropped onto grids and incubated in 2% paraformaldehyde for 20 minutes. The grids were transferred to a wax strip and washed with 100 µl PBS. The grids were incubated in 50 mmol/l glycine/PBS for 5 minutes and blocked in 5% bovine serum albumin/PBS for 10 minutes in presence or absence of 0.1% saponin. The grids were washed twice in PBS and incubated with 6-nm or 10-nm streptavidin immune-gold particles diluted 1:10 to 1:20 in 0.5% bovine serum albumin/PBS for 1 hour in presence or absence of 0.1% saponin. The grids were washed three times in PBS and incubated in 1% glutaraldehyde for 5 minutes. Following eight washes with water of 2 minutes each, the grids were incubated in uranyl oxalate for 5 minutes, and then in a 9:1 solution of 1% methyl cellulose and 4% uranyl acetate for 10 minutes on ice. Excess liquid was removed with a filter paper and the grids were air-dried for 5–10 minutes. Exosomes were examined in a JEOL 1100 transmission electron microscope (JEOL, Peabody, MA) at 60 kV, and images were obtained with an AMT digital camera (Advanced Microscopy Techniques, Woburn, MA). The number of exosomes with gold particles on the outside and inside of the exosome, as well as the total number of exosomes per field (6.83 µm^2), were counted for each condition ($n = 1,593$ exosomes in 16 fields for biotinylated hsiRNA; $n = 1,234$ exosomes in 15 fields for unloaded exosomes). The percent of exosomes with streptavidin gold particles per field was determined.

Statistical analysis. Data were analyzed using GraphPad Prism 6, version 6.04 (GraphPad Software Inc., La Jolla, CA).

In *in vitro* silencing experiments, the IC_{50} values were determined by fitting dose–response curve using "log(inhibitor) versus response—variable slope (four parameters)" equation. The bottom of the curve was set to be no less than zero and the top of the curve was set to be no >100.

The hsiRNA *in vivo* distribution data, monitored using PNA assay, were analyzed using a nonparametric Kruskal–Wallis test. The mean of each column was compared to the mean of the corresponding aCSF control column. For each mouse experiment, the level of silencing at each hsiRNA dose was normalized to the mean of the control group—the noninjected side in those mice treated with aCSF. *In vivo* silencing data were analyzed using the one-way analysis of variance test (Bonferroni's

test for multiple comparisons). The mean of each column was compared to the mean of the corresponding hsiRNA^{NTC}-exosome control column. *In vivo* innate immune response data were analyzed with an unpaired *t*-test. Differences in all comparisons were considered significant at *P* values <0.05.

SUPPLEMENTARY MATERIAL

Figure S1. Exosome purification and characterization.

Figure S2. Cholesterol is necessary for efficient loading and interaction of hsiRNAs into exosomes.

Figure S3. Electron microscopy validates presence of hsiRNAs at the surface and in the lumen of exosomes.

Figure S4. Efficient internalization of PKH67-labeled exosomes and Cy3-hsiRNAs in primary cortical neurons.

Figure S5. Concentration dependent silencing of huntingtin protein by hsiRNAHTT-loaded exosomes in primary cortical neurons.

Figure S6. Injection of exosomes and hsiRNAHTT-loaded exosomes have a slight impact on innate immune response in vivo.

Figure S7. Pump implantation for the infusion of exosomes and hsiRNA-loaded exosomes have no statistically significant impact on innate immune response *in vivo*.

Figure S8. Exosomes and hsiRNAHTT-loaded exosomes have no impact on cell viability in vivo.

Table S1. hsiRNAHTT-loaded exosomes induce bilateral Htt mRNA silencing in vivo in mouse brain.

REFERENCES

1. HD Consortium (1993). A novel gene containing a trinucleotide repeat that is expanded and unstable on Huntington's disease chromosomes. *Cell* **72**: 971–983.
2. Ross, CA and Tabrizi, SJ (2011). Huntington's disease: from molecular pathogenesis to clinical treatment. *Lancet Neurol* **10**: 83–98.
3. Warby, SC, Graham, RK and Hayden, MR (2010). *Huntington Disease. GeneReviews*™. <http://www.ncbi.nlm.nih.gov/books/NBK1305/>.
4. Boudreau, RL, McBride, JL, Martins, I, Shen, S, Xing, Y, Carter, BJ *et al.* (2009). Nonallele-specific silencing of mutant and wild-type huntingtin demonstrates therapeutic efficacy in Huntington's disease mice. *Mol Ther* **17**: 1053–1063.
5. Kordasiewicz, HB, Stanek, LM, Wancewicz, EV, Mazur, C, McAlonis, MM, Pytel, KA *et al.* (2012). Sustained therapeutic reversal of Huntington's disease by transient repression of huntingtin synthesis. *Neuron* **74**: 1031–1044.
6. Harper, SQ, Staber, PD, He, X, Eliason, SL, Martins, IH, Mao, Q *et al.* (2005). RNA interference improves motor and neuropathological abnormalities in a Huntington's disease mouse model. *Proc Natl Acad Sci USA* **102**: 5820–5825.
7. Sah, DW and Aronin, N (2011). Oligonucleotide therapeutic approaches for Huntington disease. *J Clin Invest* **121**: 500–507.
8. Stalder, L, Heusermann, W, Sokol, L, Trojer, D, Wirz, J, Hean, J *et al.* (2013). The rough endoplasmatic reticulum is a central nucleation site of siRNA-mediated RNA silencing. *EMBO J* **32**: 1115–1127.
9. Coelho, T, Adams, D, Silva, A, Lozeron, P, Hawkins, PN, Mant, T *et al.* (2013). Safety and efficacy of RNAi therapy for transthyretin amyloidosis. *N Engl J Med* **369**: 819–829.
10. Nair, JK, Willoughby, JL, Chan, A, Charisse, K, Alam, MR, Wang, Q *et al.* (2014). Multivalent N-acetylgalactosamine-conjugated siRNA localizes in hepatocytes and elicits robust RNAi-mediated gene silencing. *J Am Chem Soc* **136**: 16958–16961.
11. Rajeev, KG, Zimmermann, T, Manoharan, M, Maier, M, Kuchimanchi, S and Charisse, K (2014). RNAi agents, compositions and methods of use thereof for treating transthyretin (TTR) associated diseases Patent application #PCT/US2012/065691; Alnylam Pharmaceuticals.
12. Byrne, M, Tzekov, R, Wang, Y, Rodgers, A, Cardia, J, Ford, G *et al.* (2013). Novel hydrophobically modified asymmetric RNAi compounds (sd-rxRNA) demonstrate robust efficacy in the eye. *J Ocul Pharmacol Ther* **29**: 855–864.
13. Geary, RS, Norris, D, Yu, R and Bennett, CF (2015). Pharmacokinetics, biodistribution and cell uptake of antisense oligonucleotides. *Adv Drug Deliv Rev* **87**: 46–51.
14. Alterman, JF, Hall, LM, Coles, A, Hassler, MR, Didiot, M-C, Chase, K, *et al.* (2015). Hydrophobic siRNAs silence huntingtin mRNA in primary neurons and mouse brain. *Mol Ther Nucleic Acid* (in press).
15. Muralidharan-Chari, V, Clancy, JW, Sedgwick, A and D'Souza-Schorey, C (2010). Microvesicles: mediators of extracellular communication during cancer progression. *J Cell Sci* **123**(Pt 10): 1603–1611.
16. Distler, JH, Huber, LC, Hueber, AJ, Reich, CF 3rd, Gay, S, Distler, O *et al.* (2005). The release of microparticles by apoptotic cells and their effects on macrophages. *Apoptosis* **10**: 731–741.
17. Pegtel, DM, Cosmopoulos, K, Thorley-Lawson, DA, van Eijndhoven, MA, Hopmans, ES, Lindenberg, JL *et al.* (2010). Functional delivery of viral miRNAs via exosomes. *Proc Natl Acad Sci USA* **107**: 6328–6333.
18. Wang, K, Zhang, S, Weber, J, Baxter, D and Galas, DJ (2010). Export of microRNAs and microRNA-protective protein by mammalian cells. *Nucleic Acids Res* **38**: 7248–7259.
19. Valadi, H, Ekström, K, Bossios, A, Sjöstrand, M, Lee, JJ and Lötvall, JO (2007). Exosome-mediated transfer of mRNAs and microRNAs is a novel mechanism of genetic exchange between cells. *Nat Cell Biol* **9**: 654–659.
20. El Andaloussi, S, Lakhal, S, Mäger, I and Wood, MJA (2012). Exosomes for targeted siRNA delivery across biological barriers. *Adv Drug Deliv Rev*. doi:10.1016/j.addr.2012.08.008.
21. Pan, Q, Ramakrishnaiah, V, Henry, S, Fouraschen, S, de Ruiter, PE, Kwekkeboom, J *et al.* (2012). Hepatic cell-to-cell transmission of small silencing RNA can extend the therapeutic reach of RNA interference (RNAi). *Gut* **61**: 1330–1339.
22. Kooijmans, SA, Vader, P, van Dommelen, SM, van Solinge, WW and Schiffelers, RM (2012). Exosome mimetics: a novel class of drug delivery systems. *Int J Nanomedicine* **7**: 1525–1541.
23. Lässer, C (2012). Exosomal RNA as biomarkers and the therapeutic potential of exosome vectors. *Expert Opin Biol Ther* **12 (Suppl 1)**: S189–S197.
24. Lee, Y, El Andaloussi, S and Wood, MJ (2012). Exosomes and microvesicles: extracellular vesicles for genetic information transfer and gene therapy. *Hum Mol Genet* **21**(R1): R125–R134.
25. Marcus, ME and Leonard, JN (2013). FedExosomes: engineering therapeutic biological nanoparticles that truly deliver. *Pharmaceuticals (Basel)* **6**: 659–680.
26. Nazarenko, I, Rupp, AK and Altevogt, P (2013). Exosomes as a potential tool for a specific delivery of functional molecules. *Methods Mol Biol* **1049**: 495–511.
27. Zomer, A, Vendrig, T, Hopmans, ES, van Eijndhoven, M, Middeldorp, JM and Pegtel, DM (2010). Exosomes: fit to deliver small RNA. *Commun Integr Biol* **3**: 447–450.
28. El-Andaloussi, S, Lee, Y, Lakhal-Littleton, S, Li, J, Seow, Y, Gardiner, C *et al.* (2012). Exosome-mediated delivery of siRNA *in vitro* and *in vivo*. *Nat Protoc* **7**: 2112–2126.
29. Alvarez-Erviti, L, Seow, Y, Yin, H, Betts, C, Lakhal, S and Wood, MJ (2011). Delivery of siRNA to the mouse brain by systemic injection of targeted exosomes. *Nat Biotechnol* **29**: 341–345.
30. Bryniarski, K, Ptak, W, Jayakumar, A, Püllmann, K, Caplan, MJ, Chairoungdua, A *et al.* (2013). Antigen-specific, antibody-coated, exosome-like nanovesicles deliver suppressor T-cell microRNA-150 to effector T cells to inhibit contact sensitivity. *J Allergy Clin Immunol* **132**: 170–181.
31. Saryier, I (2013). Transfection of neuronal cultures. *Methods Mol Biol* **1078**: 133–9.
32. Nallagatla, SR and Bevilacqua, PC (2008). Nucleoside modifications modulate activation of the protein kinase PKR in an RNA structure-specific manner. *RNA* **14**: 1201–1213.
33. Théry, C, Amigorena, S, Raposo, G and Clayton, A (2006). Isolation and characterization of exosomes from cell culture supernatants and biological fluids. *Curr Protoc Cell Biol* **Chapter 3**: Unit 3.22: 3.22.1-3.22.29.
34. Roehl, I, Schuster, M and Seiffert, S (2011). Oligonucleotide detection method using a peptide nucleic acid probe. Patent application #CA 2739672; Axolabs Gmbh.
35. Imai, Y, Ibata, I, Ito, D, Ohsawa, K and Kohsaka, S (1996). A novel gene iba1 in the major histocompatibility complex class III region encoding an EF hand protein expressed in a monocytic lineage. *Biochem Biophys Res Commun* **224**: 855–862.
36. Tetta, C, Ghigo, E, Silengo, L, Deregibus, MC and Camussi, G (2013). Extracellular vesicles as an emerging mechanism of cell-to-cell communication. *Endocrine* **44**: 11–19.
37. Cooper, JM, Wiklander, PB, Nordin, JZ, Al-Shawi, R, Wood, MJ, Vithlani, M *et al.* (2014). Systemic exosomal siRNA delivery reduced alpha-synuclein aggregates in brains of transgenic mice. *Mov Disord* **29**: 1476–1485.
38. Ohno, S, Takanashi, M, Sudo, K, Ueda, S, Ishikawa, A, Matsuyama, N *et al.* (2013). Systemically injected exosomes targeted to EGFR deliver antitumor microRNA to breast cancer cells. *Mol Ther* **21**: 185–191.

39. Kosaka, N, Iguchi, H, Yoshioka, Y, Hagiwara, K, Takeshita, F and Ochiya, T (2012). Competitive interactions of cancer cells and normal cells via secretory microRNAs. *J Biol Chem* **287**: 1397–1405.

40. Mizrak, A, Bolukbasi, MF, Ozdener, GB, Brenner, GJ, Madlener, S, Erkan, EP *et al.* (2013). Genetically engineered microvesicles carrying suicide mRNA/protein inhibit schwannoma tumor growth. *Mol Ther* **21**: 101–108.

41. Kooijmans, SA, Stremersch, S, Braeckmans, K, de Smedt, SC, Hendrix, A, Wood, MJ *et al.* (2013). Electroporation-induced siRNA precipitation obscures the efficiency of siRNA loading into extracellular vesicles. *J Control Release* **172**: 229–238.

42. Maday, S, Twelvetrees, AE, Moughamian, AJ and Holzbaur, EL (2014). Axonal transport: cargo-specific mechanisms of motility and regulation. *Neuron* **84**: 292–309.

43. Cattaneo, E, Rigamonti, D, Goffredo, D, Zuccato, C, Squitieri, F and Sipione, S (2001). Loss of normal huntingtin function: new developments in Huntington's disease research. *Trends Neurosci* **24**: 182–188.

44. Dragatsis, I, Levine, MS and Zeitlin, S (2000). Inactivation of Hdh in the brain and testis results in progressive neurodegeneration and sterility in mice. *Nat Genet* **26**: 300–306.

45. Broering, R, Real, CI, John, MJ, Jahn-Hofmann, K, Ickenstein, LM, Kleinehr, K *et al.* (2014). Chemical modifications on siRNAs avoid Toll-like-receptor-mediated activation of the hepatic immune system *in vivo* and *in vitro*. *Int Immunol* **26**: 35–46.

46. D'Asti, E, Chennakrishnaiah, S, Lee, TH and Rak, J (2016). Extracellular vesicles in brain tumor progression. *Cell Mol Neurobiol* **36**: 383–407.

47. Hassani, Z, O'Reilly, J, Pearse, Y, Stroemer, P, Tang, E, Sinden, J *et al.* (2012). Human neural progenitor cell engraftment increases neurogenesis and microglial recruitment in the brain of rats with stroke. *PLoS One* **7**: e50444.

48. Vishnubhatla, I, Corteling, R, Stevanato, L, Hicks, C and Sinden, J (2014). The Development of stem cell-derived exosomes as a cell-free regenerative medicine. *J Circ Biomarkers*: 3:2: 1–14. doi:10.5772/58597.

49. Bonafede, R, Scambi, I, Peroni, D, Potrich, V, Boschi, F, Benati, D *et al.* (2016). Exosome derived from murine adipose-derived stromal cells: neuroprotective effect on *in vitro* model of amyotrophic lateral sclerosis. *Exp Cell Res* **340**: 150–158.

50. Shelke, GV, Lässer, C and Lötvall, J (2014). Contribution of FBS-derived RNA in cell cultures and comparison of different FBS depletion protocols. *Int Meet ISEV Rotterdam* **3**: 136.

51. International Society for Extracellular Vesicles (2014). Minimal experimental requirements for definition of extracellular vesicles and their functions: a position statement from the International Society for Extracellular Vesicles. *J Extracell Vesicles* **3**: 26913.

52. DiFiglia, M, Sapp, E, Chase, K, Schwarz, C, Meloni, A, Young, C *et al.* (1995). Huntingtin is a cytoplasmic protein associated with vesicles in human and rat brain neurons. *Neuron* **14**: 1075–1081.